Overview of recent results from the Tore Supra ECE diagnostics

M.Talvard, W.D.Liu, G.Giruzzi

Association Euratom-CEA sur la Fusion
Centre d'Etudes de Cadarache
13108 Saint Paul-lez-Durance (FRANCE)

Abstract The Tore Supra ECE diagnostic system consists of a set of 3 Michelson and 12 Fabry-Perot interferometers, which is now fully operational. We present results obtained with the 3 Michelson during LHCD experiments first. It is shown how the sensitivity of the diagnostic to rather high $v_\perp$ prevents detection of $v_{//}$ anisotropies. On the other hand, measurements during the Ohmic phase reveal some unexpected anisotropy which can be attributed to superthermal electrons related to the bootstrap current. The 12 Fabry-Perot have been operated using high acquisition sampling rates during pellet injection experiments. A shudder preceding the pellet itself is clearly evidenced just before an internal disruption occurs. During sawtooth activity, such measurements are also used to study the dynamics of the m=1, n=1 instability on the q = 1 surface itself.

1. Diagnostic installation

The Tore Supra ECE diagnostic is located outside the torus hall, 30 metres away from the plasma chamber. The coupling line is composed of 15 antennae looking in the equatorial plane and in the poloidal plane (fig.1) coupled to oversized waveguides by means of wedged fused quartz windows. Each line includes a polarizer to select for X or O radiation mode, a mode filter used both to reduce the diagnostic antenna pattern and to provide mechanical and electrical insulation from the machine. Reflectors mounted on benches have been adjusted using a telescope aiming at a target through the waveguides.

The Tore Supra Michelson interferometers provide routinely one electron cyclotron spectrum in the range 50 - 1000 GHz every 22 ms with a spatial resolution of 12 cm along the line of sight, i.e radially. In Situ calibration using a black body source (800 K - extended area) is performed once a year. A total integration time of 10 hours per Michelson has been necessary to provide T_e profiles such as shown in fig.2. An analysis program installed on workstation is able to store the $T_e(R,t)$ matrix shot after shot in a processed data base.

The 12 Fabry Perot interferometers are routinely used in static mode in order to follow the temporal evolution of the spectrum intensity at a given frequency. The spatial resolution along the line of sight is 10 cm , well adapted to observe large MHD modes such as (m=1, n=1) or (m=2, n=1). They can be operated simultaneously using standard (Δt = 1 ms - whole shot) and fast ($\Delta t \geq 1$ µs - 32000 data points) acquisition modules. An analysis program installed on workstation achieves calibration by comparison with the Michelson processed data and stores the six standard temporal evolutions corresponding to the equatorial views in the data base. An example of processed data is given in fig.3.

2. Michelson spectra during LHCD experiments

Electron cyclotron non thermal spectra obtained on the Michelson $M_\perp$ viewing perpendicularly to the magnetic field during RF assisted discharges are reported on fig.4 and 5 as a function of the RF power and the plasma average density, respectively. The ECE spectrum is mainly composed of both the thermal levels and the downshifted non thermal components of the three first harmonics of the cyclotron frequency. We shall concentrate on the second harmonic only since the first one - whose interpretation is more ambiguous - has been truncated. As expected, the 2nd harmonic non thermal intensity is increasing with the RF power and decreasing with the plasma density. Moreover, the peak position is independent of the RF power. Surprisingly the intensity, the width and the position of this peak are rather insensitive to variations of $n_{//}$ of the launched waves, and thus of the energy of the non thermal electrons. When looking at the three Michelson spectra measured with P_{RF}= 3 MW and $\langle n_e \rangle = 2.1\ 10^{19}\ m^{-3}$ (fig.6), it appears that neither the peak position nor the peak width is depending on the Michelson view. In principle, according to the resonance condition :

$$\omega = \frac{\omega_c}{\gamma} + k_{//} v_{//}$$

where ω_c is the cyclotron frequency, γ the relativistic correction to the electron mass, $k_{//}$ the parallel component of the wave number and $v_{//}$ the parallel velocity of the emitting electron, one would expect some anisotropy between the two oblique lines of sight when the plasma current is carried by high $v_{//}$ electrons. Indeed, the Doppler term $k_{//}v_{//}$ takes opposite signs for the two Michelson views so called M_{Bs} for "blue-shifted" since $k_{//}v_{//} > 0$ and M_{Rs} for "red-shifted" since $k_{//}v_{//} < 0$. It is possible to show that the shape of the 2nd harmonic non thermal peak is mainly determined by the plasma density.

In fact, the above mentioned parametric dependence can be easily interpreted by introducing the X-mode upper hybrid cut-off layer between the two first thermal harmonics. As a consequence, the 2nd harmonic non thermal peak is no longer representative of the energy extent of the electron tail. Moreover, the peak position is not associated with the mean energy $\langle E_{st} \rangle$ of the supra-thermal distribution. One can deduce that $\langle E_{st} \rangle$ is greater than 250 keV for most experiments.

Even introducing the upper hybrid cut-off layer in order to explain the global features, a remaining anisotropy should be observed between $M_\perp$, M_{Rs} and M_{Bs}. The lack of significant asymmetry can be understood by taking into account the weighting of the measurement technique.

In fact, ECE is maximum for a given electron energy when $v_\perp > v_{//}$. The shaded region in fig.7 has been proved to be at the origin of more than 90% of the total measured ECE. Fokker Planck calculation of the distribution function for a plasma with $<n_e> = 3\ 10^{19}\ m^{-3}$ and $P_{RF} = 4$ MW is also reported in fig.7. It appears that $v_{//}$ anisotropies due to RF power are not detectable by such an ECE antenna.

There is a last point to be discussed concerning ECE spectra during LHCD experiments. It concerns T_e measurements deduced from the 2nd thermal harmonic. As previously seen, the 2nd harmonic thermal emission will be here superimposed to the downshifted 2nd harmonic non thermal component partly reabsorbed by the plasma bulk and the downshifted 3rd harmonic non thermal emission. Spectra shape analysis show that the non thermal intensity is sharply decreasing with the harmonic number. Even at low densities, i.e $<n_e> < 2\ 10^{19}\ m^{-3}$ for which the non thermal effects are larger, the parasitic power due to the downshifted 3rd harmonic is of the order of 10% of the T_e intensity. This is not compatible with theoretical expectations that give an intensity of the same order than T_e. On the other hand, the calculated optical depth at R = 2.4 m is ≈ 40. The 2nd harmonic non thermal contribution is hence reduced by a factor e^{-40} near the plasma center. In conclusion, T_e measurements deduced from ECE in presence of hybrid power remains valid in most cases in the central part of the plasma. This has been confirmed elsewhere by the Thomson scattering diagnostic showing a good agreement between the two $T_e(R)$ measurements for densities as low as $2\ 10^{19}\ m^{-3}$.

3. Michelson spectra during Ohmic discharges

The Michelson interferometers have been operated during Ohmic phases, in order to check for the absolute calibration of the three lines. It is remarkable that both the absolute level and the general shape of the spectra are very similar all over the frequency band, except for M_{Bs} which is significantly higher than the thermal level in the 2nd-3rd harmonics overlapping region (fig.8). A statistical study using more than 20 toroidal magnetic fields between 3 and 4 T confirmed this last point.

As previously presented /1/, it is necessary to introduce a small anisotropy in the distribution function in order to account for these observations. It has been shown that such anisotropy has to be located in the high $v_\perp$ region of the velocity space in order to be detected by the ECE antennae. One of the most favourable effect proposed is the detrapping of banana particles which originates the bootstrap current. According to a recent bootstrap scaling in tokamaks /2/ :

$$\frac{I_{boot}}{I_p} = \sqrt{\varepsilon}\ \beta_p\ F$$

where ε is the tokamak inverse aspect ratio, β_p the poloidal beta and F a shaping factor depending on the peaking of the pressure, temperature and current profiles. The factor F is particularly expected to decrease with the peaking α_T of the temperature profile. The results shown in fig.9 and 10 seem to confirm this interpretation.

4. Fabry Perot measurements during pellet injection experiments

A centrifuge pellet fueling system /3/ together with a high speed pellet injector /4/ have been installed on Tore Supra in order to control the plasma density during long pulses (> 10 s) and to study the ablation physics. Six Fabry Perot cavities have been adjusted in order to look at r = 0., .15, .30, .40, .50 and .65 m in the equatorial plane for a plasma minor radius of .78 m. Fig.11a shows standard $T_e(r)$ evolutions and fig.11b an expanded view of the fast acquisition modules around the pellet event at 6.16 s. Experiments with pellet velocities in the range 500 - 2300 ms^{-1} have been performed. ECE observations can be summerized as follows :

Two distinct phases have to be considered during the temperature drop due to the pellet. First is a fast propagation of a "shudder" as soon as the pellet enters the plasma. The propagation time between two extreme views is close to 40 µs corresponding to a velocity between 10 and 15 kms^{-1}. This velocity is independent on the pellet velocity. The temperature drop during this first phase is close to 10% for all radii within the half plasma radius and approximately 40% outside. The second phase is characterised by a sawtooth-like behaviour on the ECE channels. For this particular shot, it is triggered approximately 200 µs after the pellet had entered the plasma. It seems to be associated with the pellet reaching a given magnetic surface near the mid-plasma radius. After the disruption, the relative temperature drop is more or less constant, namely 75% on all radii.

The trigger mechanism observed could be understood either as a modification of the profiles which would destabilize MHD modes, or a turbulent mechanism associated with the pellet. The time constant of 200 µs, small compared to MHD characteristic times (order of ms^{-1}) tends to credit the latter interpretation.

5. Fabry Perot measurements during sawtooth activity

Fast acquisition modules have been first installed in order to look at the radial propagation of heat pulses during sawtooth activity. Fig.12a represents the temporal evolution of 5 Fabry Perot lines viewing in the equatorial plane at r = -.10, 0., .10, .20, .35 m. The last signal corresponds to the heat pulse propagating outside the q = 1 surface which is localised around r = .20 m. The total time on fig.12a is 2 ms, while the collapse duration is 150 µs, which is particularly long by comparison with more usual sawteeth (typically 100 µs). This particular example for a plasma with additional heating has been reported because it shows very clearly the rotation of a hot spot during the crash. More generally, two distinct situations have been observed. When there is no visible precursor to the disruption, namely no detected oscillation at a frequency close to 1 kHz around the q = 1 surface, one observes the sudden rotation of a hot core growing on a time scale of a few ms and terminated by a crash, such as shown in fig. 12a. The rotation velocity of the plasma core is close to 1 kHz before the crash. During the crash, the observation is compatible with a rapid rotation of this hot core of half a turn at a frequency of 10 kHz. This could be attributed to the remaining confined plasma around the original magnetic axis, which would have been compressed by a growing instability on the q = 1 surface. A second situation has been observed when there is a clear evidence for a saturated precursor

with a poloidal symmetry m = 1, 10 ms or even more before the collapse. The latter is particularly visible on the q = 1 surface, i.e 0.25 m in our case. Although the instability has reached a saturated level, the disruption occurs without detection of any hot spot as previously. The measured frequency of the rotating mode is in the range 1 - 1.5 kHz. The collapse time is again close to 100 μs.

To give a more precise idea of the sawtooth phenomenon, we have adjusted the Fabry Perot cavities in the poloidal plane, in order to visualize the q = 1 surface. Five lines of sight have been operated as reported on fig. 12b. The total time on fig.12b is 32 ms. The disruption occurs at mid time near t = 4.08 s. We observe a hot spot on the fourth channel, although the m = 1 saturated mode has disappeared 5 ms before. Analysis of the m = 1 phasing on q = 1 proves that the rotation occurs in the electron diamagnetic direction (in all measured cases). This m = 1 activity is observed again 5 ms after the crash showing that the q = 1 surface is always present in the plasma. Again, the rotation velocity of this mode is close to 1 kHz. The two external views (top and bottom of the fig.12b) correspond to a plasma minor radius of r = .35 m and are probably looking outside the q = 1 surface since a heat pulse has been detected. Due to the rotation direction, the hot spot appearing on the fourth channel is no more visible on the upper channels since it has been expelled in less than half a turn.

Combined observations of both the radial propagation and the q = 1 surface have also been obtained. Fig.13a-b show an expanded view corresponding to 2 ms for the same event around t = 4.256 s. The usual behaviour of the temperature collapse is visible on the horizontal views with a heat pulse propagating outside the plasma minor radius r = .35 m (fig.13a). Measurements on the q = 1 surface (fig.13b) shows evidence of rotation in the electron diamagnetic direction of the hot plasma core, followed by a trail at a temperature lower than that of the surrounding plasma during the disruption. The deep hole visible on the fourth channel is followed by the residual plasma core after one poloidal turn (the collapsing core is visible on the second and third channels). The coherency between all these measurements indicates or can be interpreted in the following manner :

i) There is a magnetic perturbation with an m = 1 symmetry on the q = 1 surface. This one leads more often to a tearing mode. When it is detectable, the measured poloidal velocity is close to 1 kHz in the electron diamagnetic direction.

ii) When the instability grows around q = 1, the plasma core corresponding to the original nested magnetic surfaces around the magnetic axis is being compressed. In the same time, the magnetic turbulence intrinsic to the mode creates a partial stochastization of the q = 1 surface, which becomes broader. It could explain why temperature fluctuations on the q = 1 surface are no more detectable.

iii) For a given stochasticity threshold, a thermal pumping from the cold to the hot part of the magnetic structure is triggered. The thermal pumping is initiated as well as some energy is delivered to the system. The nature of this energy is still under investigation. When the thermal load is too large for the ergodized surface, a few ms later, the disruption occurs. The hot spot is expelled outside q = 1 through the X point preferentially accompanied by a rotation in the electron diamagnetic direction at a frequency 10 times larger than the precursor one.

iv) After the disruption, a new thermal equilibrium is reached in which the q = 1 surface , always stochastic during the first ms, recovers progressively a strong magnetic structure. This is understandable because the turbulence has been stabilized since the hot core is no more present. At this moment the mode can be detected again.

5. Fabry Perot measurements on the q = 2 surface

The set of Fabry Perot interferometers looking in the poloidal plane has also been adjusted in order to look at the q = 2 surface during the current ramp up and the pre-disruptive phases. Very preliminary results have revealed oscillating structures with an m = 4 poloidal symmetry during the ramp up phase, which demonstrates the good sensitivity of these measurements. Further work is planned, in particular to study the locking phase of magnetic islands before disruption.

/1/ M.Talvard et al in proceedings of the joint 19th EPS - 9th ICPWIP - 9th KIEV conference, INNSBRUCK, 1992.

/2/ H.R.Wilson Nucl. Fus. 32, 257, 1992.

/3/ C.A.Foster et al and A.Geraud et al in proceedings of the 17th SOFT, ROME, 1992.

/4/ J.P.Perin et al and A.Geraud et al in proceedings of the 17th SOFT, ROME, 1992.

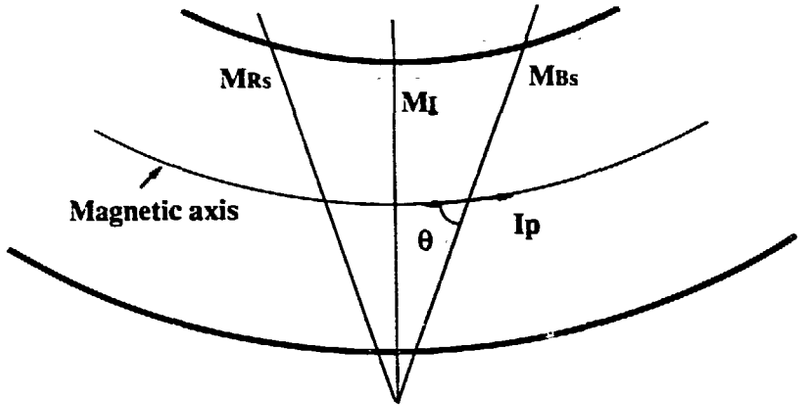

Equatorial view of the Michelson lines of sight

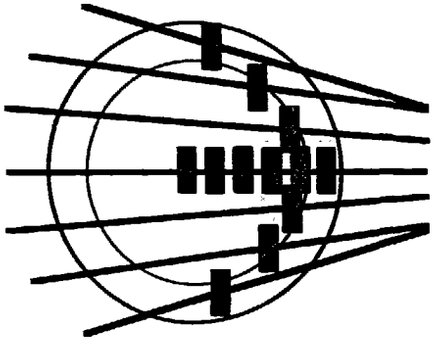

Poloidal view of the Fabry Perot lines of sight

Fig.1 The Tore Supra ECE diagnostic antenna

Example of ECE processed data for shot 8871

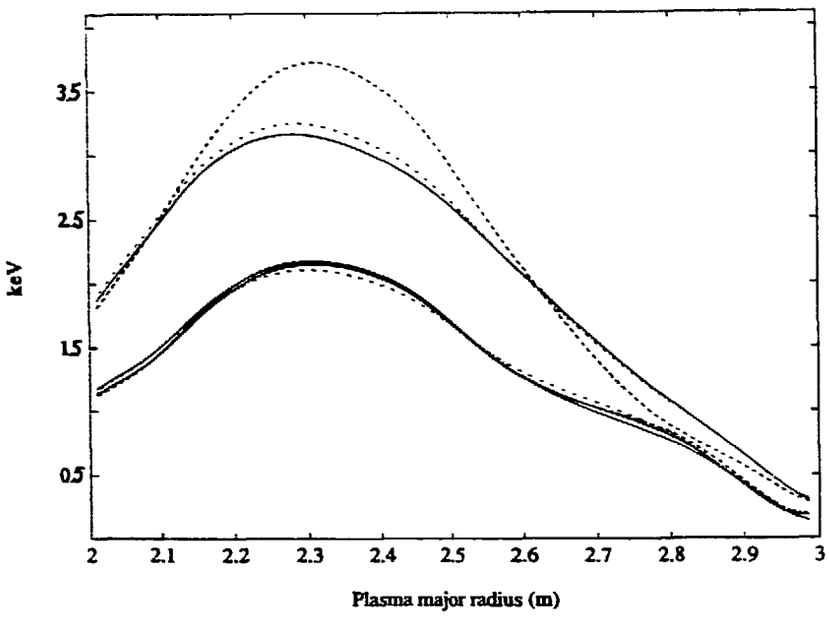

Fig.2 Michelson T_e profiles during the Ohmic phase and during a sawtooth with 3.5 MW ICRH.

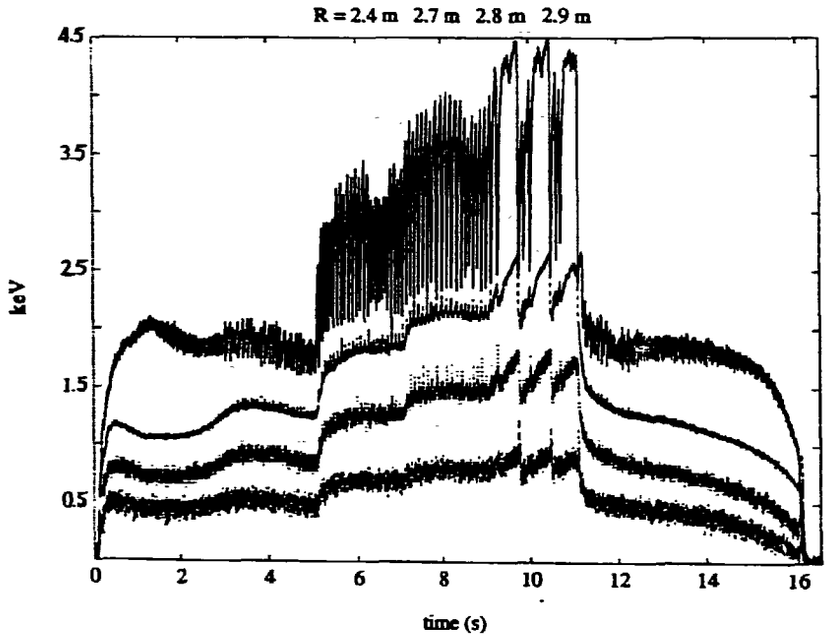

Fig.3 Fabry Perot T_e evolutions for 4 plasma radii in the equatorial plane

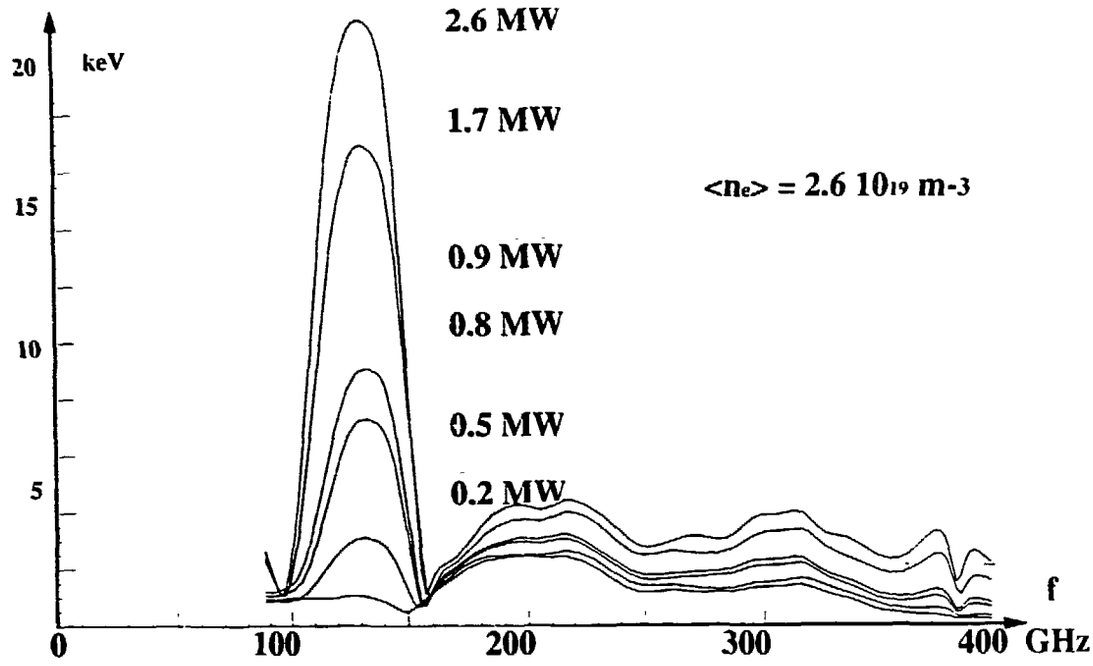

Fig.4 ECE spectra measured on $M_{\perp}$ (RF power dependence)

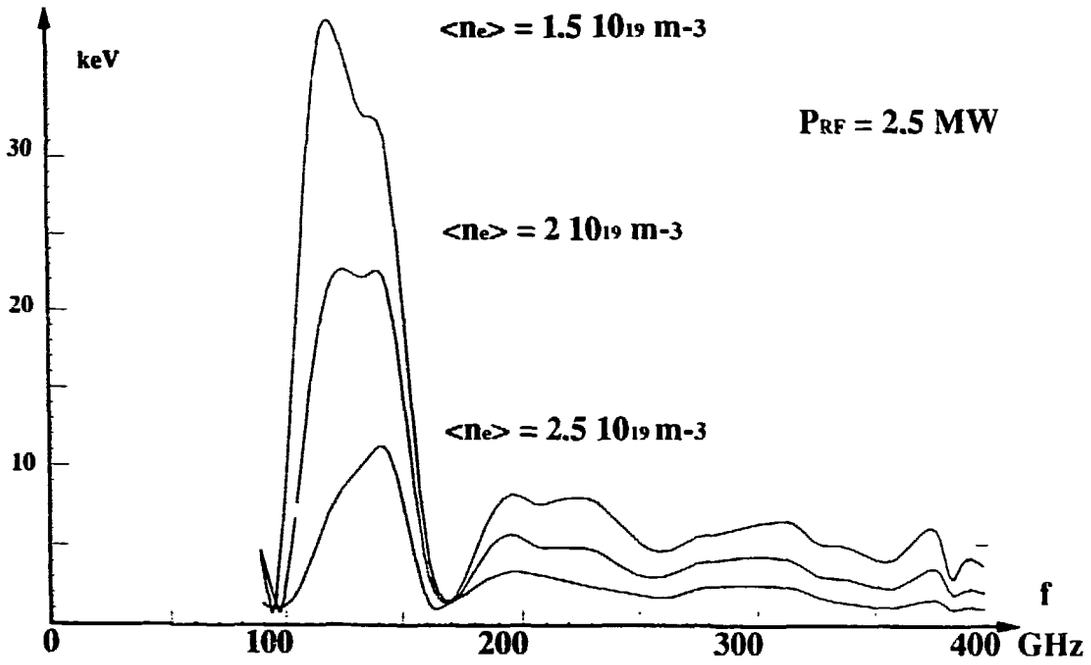

Fig.5 ECE spectra measured on $M_{\perp}$ (density dependence)

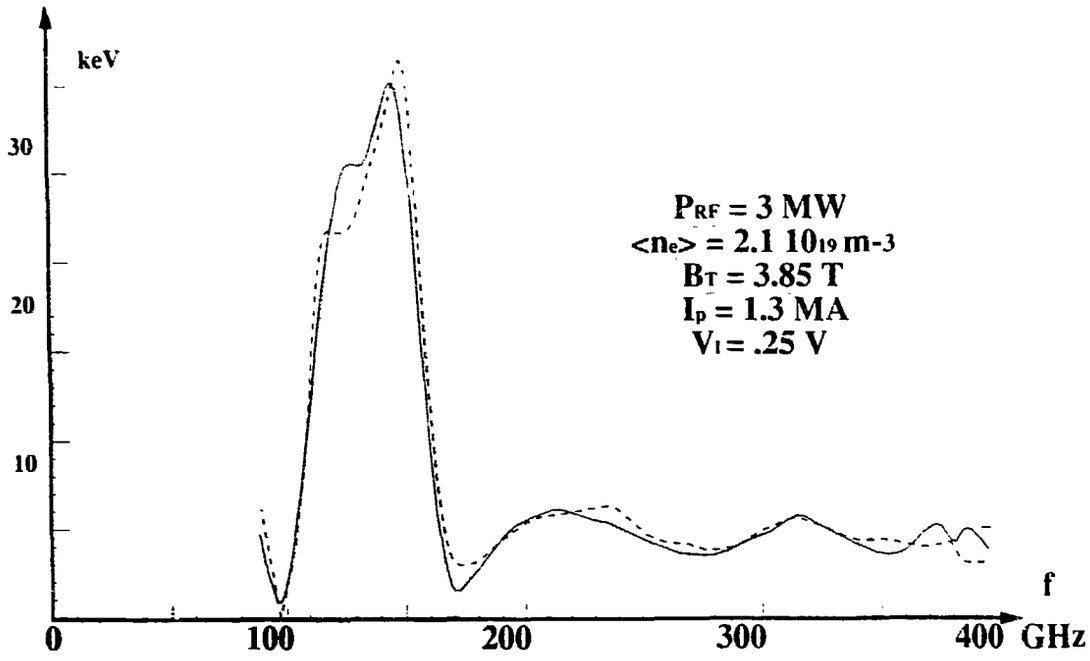

Fig.6 ECE spectra measured on M_{B_s} (dashed), $M_{\perp}$ (solid), M_{R_s} (dots)

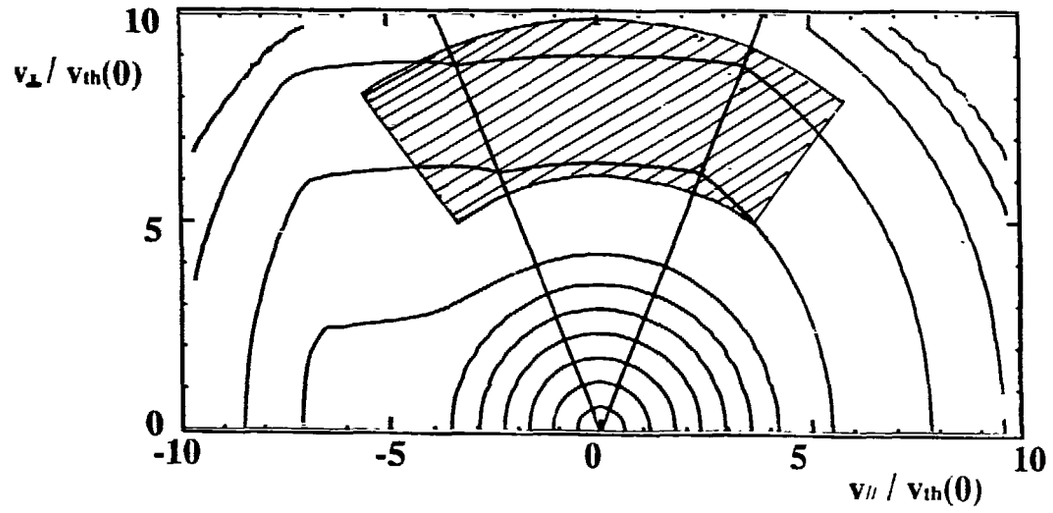

Fig.7 Fokker Planck calculation of the electron distribution function. The shaded region represents more than 90% of the measured ECE.

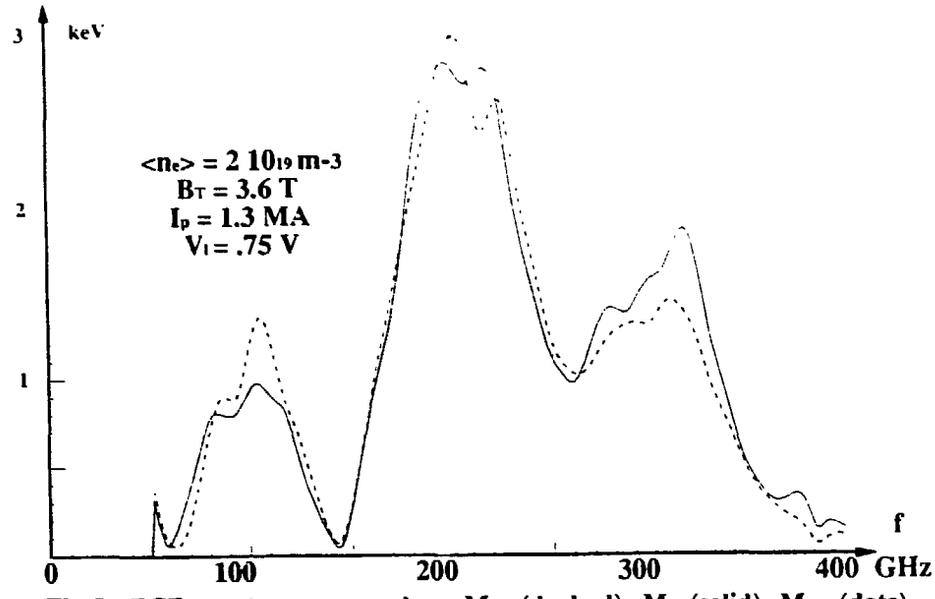

Fig.8 ECE spectra measured on M_{B_s} (dashed), $M_{\perp}$ (solid), M_{R_s} (dots)

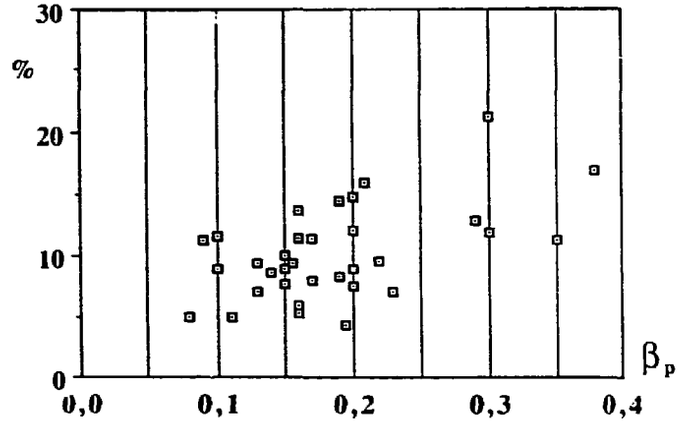

Fig.9 Anisotropy measured at half plasma radius (R = 2 m) on M_{B_s}.

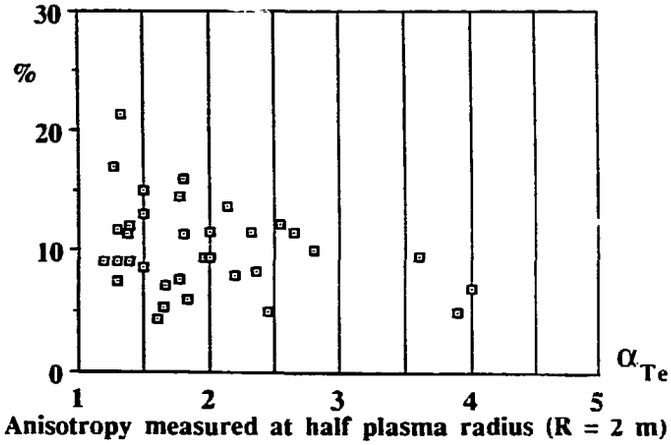

Fig.10 Anisotropy measured at half plasma radius (R = 2 m) on M_{B_s}.

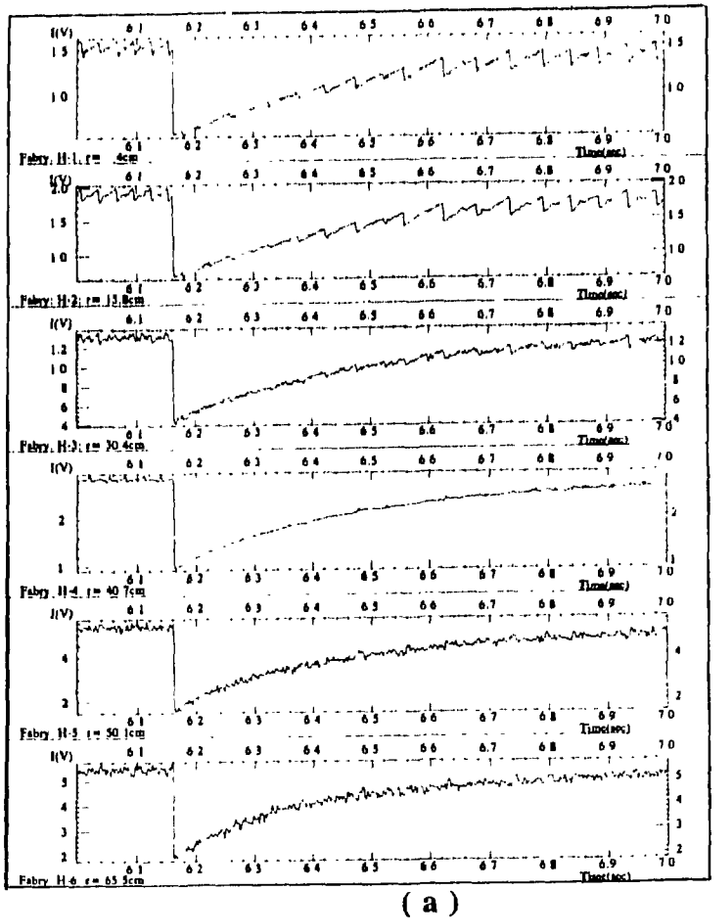

(a)

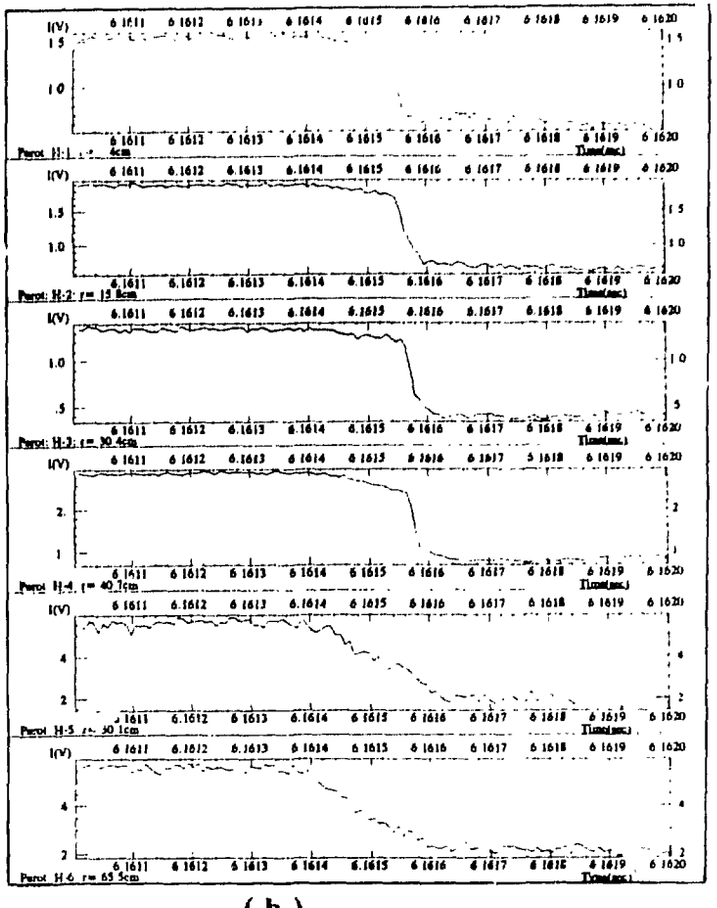

(b)

Fig.11 Standard (a) and fast (b) acquisition with the Fabry Perot interferometers during a pellet injection.

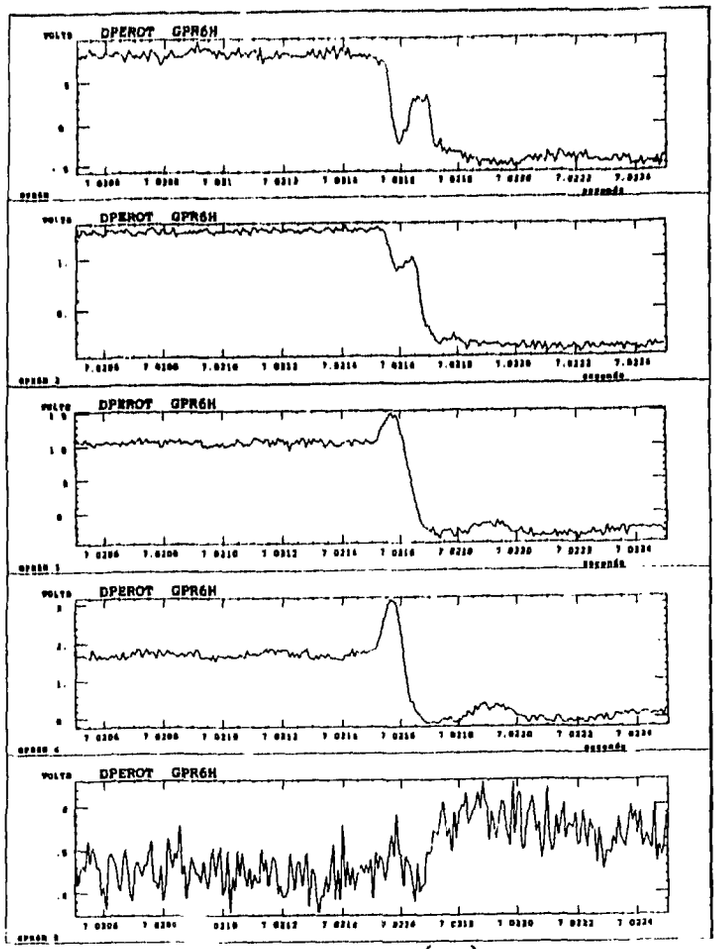

(a)

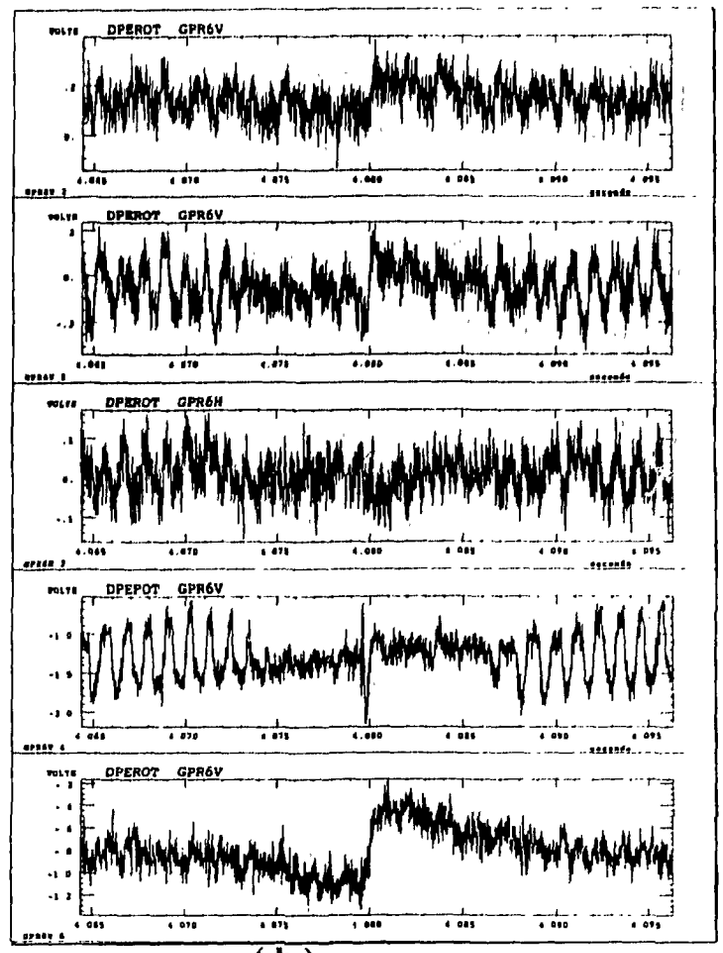

(b)

Fig.12 Fast acquisition using the Fabry Perot horizl views (a) and the vertl views looking at the q = 1 surface (b) during sawteeth.

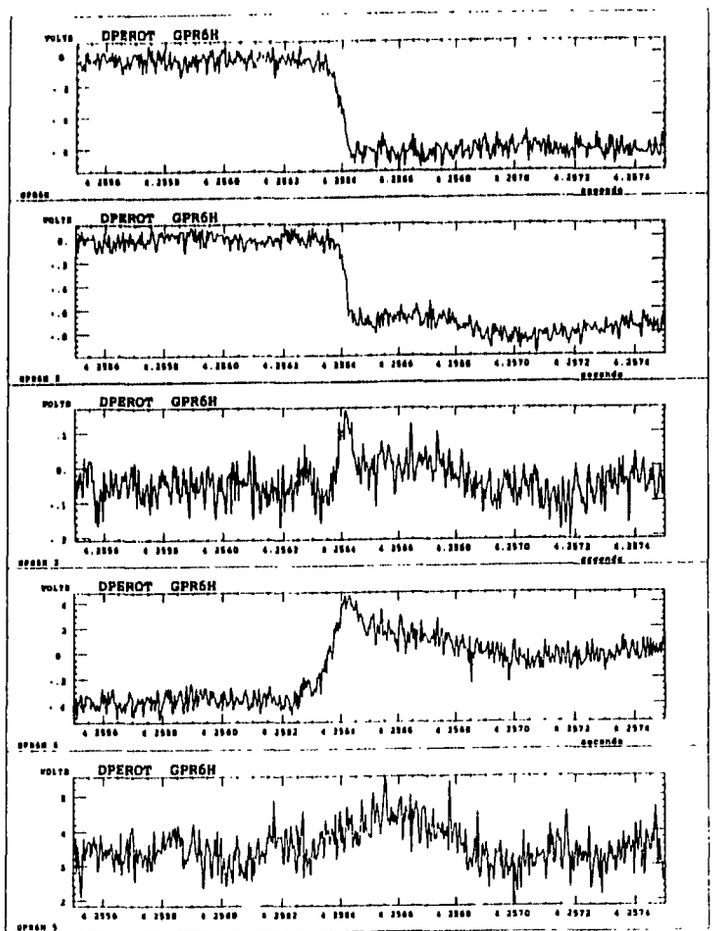

(a)

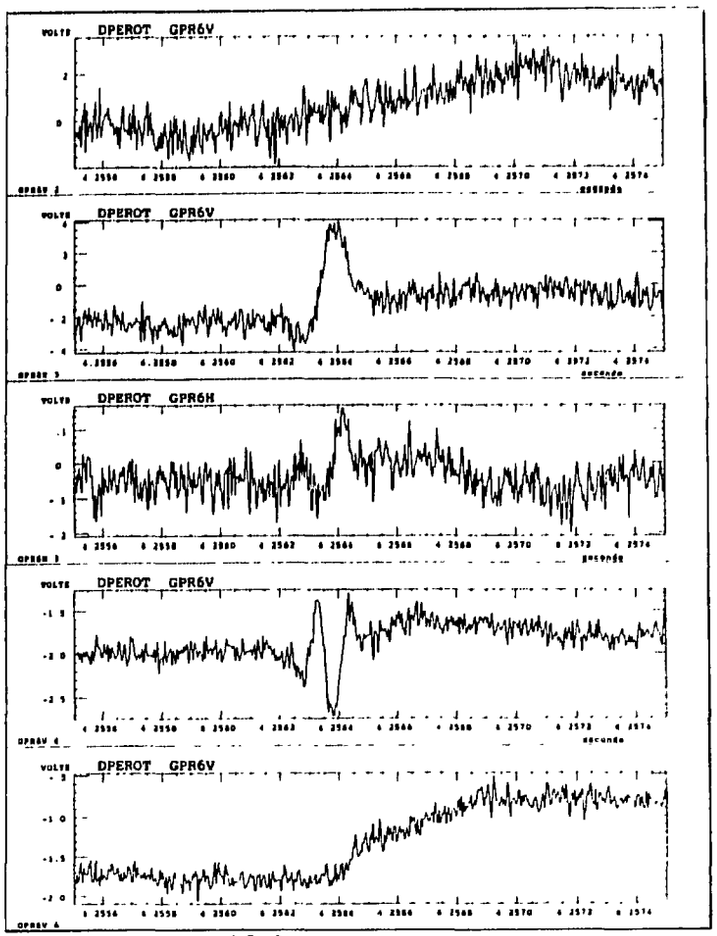

(b)

Fig.13 Fast acquisition using the Fabry Perot horizl views (a) and the vertl views looking at the q = 1 surface (b) for the same sawtooth.